THE JOURNAL OF PHYSICAL CHEMISTRY Letters

Letter

Cite This: J. Phys. Chem. Lett. 2018, 9, 3555−3560

pubs.acs.org/JPCL

Optical Control of Reactions between Water and Laser-Cooled Be^+ Ions

Tiangang Yang,*[,†] Anyang Li,*[,‡] Gary K. Chen,[†] Changjian Xie,[§] Arthur G. Suits,[∥] Wesley C. Campbell,[†] Hua Guo,[§] and Eric R. Hudson[†]

[†]Department of Physics and Astronomy, University of California, Los Angeles, Los Angeles, California 90095, United States

[‡]Key Laboratory of Synthetic and Natural Functional Molecule Chemistry, Ministry of Education, College of Chemistry and Materials Science, Northwest University, 710127 Xi'an, P. R. China

[§]Department of Chemistry and Chemical Biology, University of New Mexico, Albuquerque, New Mexico 87131, United States

[∥]Department of Chemistry, University of Missouri, Columbia, Missouri 65211, United States

Supporting Information

ABSTRACT: We investigate reactions between laser-cooled Be^+ ions and room-temperature water molecules using an integrated ion trap and high-resolution time-of-flight mass spectrometer. This system allows simultaneous measurement of individual reaction rates that are resolved by reaction product. The rate coefficient of the $Be^+(^2S_{1/2}) + H_2O \rightarrow BeOH^+ + H$ reaction is measured for the first time and is found to be approximately two times smaller than predicted by an ion−dipole capture model. Zero-point-corrected quasi-classical trajectory calculations on a highly accurate potential energy surface for the ground electronic state reveal that the reaction is capture-dominated, but a submerged barrier in the product channel lowers the reactivity. Furthermore, laser excitation of the ions from the $^2S_{1/2}$ ground state to the $^2P_{3/2}$ state opens new reaction channels, and we report the rate and branching ratio of the $Be^+(^2P_{3/2}) + H_2O \rightarrow BeOH^+ + H$ and $H_2O^+ + Be$ reactions. The excited-state reactions are nonadiabatic in nature.

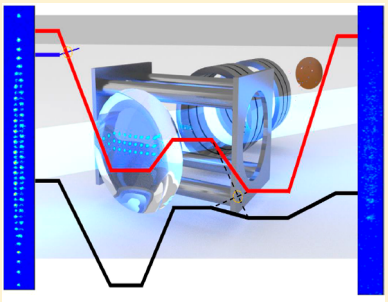

Low-temperature reactions of simple ions with small molecules play a central role in astrochemical environments from interstellar clouds to cometary comae to planetary atmospheres, including that of Earth.[1,2] The chemical evolution of interstellar molecular clouds ultimately yields the seedbed from which new stars and planets are born and the raw materials from which life likely developed. A firm understanding of the reaction rates for a host of elementary ion−molecule reactions is essential to accurately model these environments. Techniques such as selected ion flow tubes (SIFTs),[3] guided ion beams,[4] and supersonic flows (CRESU)[5] have improved our empirical understanding of these processes; however, each has its own limitations.[6,7] Theoretically, it has long been recognized that these ion−molecule reactions are often barrierless, and their rates are frequently described by capture models.[8] However, recent studies have revealed that dynamical features can sometimes prevail,[9−11] in which case statistical treatments may not be accurate.[12,13] Therefore, new experimental and theoretical efforts are needed to accurately address ion−molecule chemistry.

We have developed an approach, adapted from the ultracold ion community,[14−16] to study reactions of atomic ions with small molecules. Here we report the use of this approach to study the reaction of Be^+ with gas-phase water for the first time. There have been very few experimental studies of gas-phase reactions between metal ions and water, especially at low temperature, despite their importance for metal ion chemistry in a range of environments.[17−19]

Singly ionized beryllium is a particularly attractive metallic reactant to use for such studies because it is both theoretically tractable and experimentally highly controllable. The relatively simple electronic structure of this three-electron ion allows both highly accurate characterization of its electronic structure and laser cooling,[20] and the low mass of Be^+ lends itself to high motional frequencies as well as efficient sympathetic cooling of other chemically interesting atomic ions when employed in ion traps.[21−24] For the molecular reaction partner, H_2O is arguably the most important molecule in chemistry, and theoretical studies of its reactions with a single atom have been reported on full-dimensional potential energy surfaces (PESs).[25−29] Thus this system of reagents provides an opportunity to perform a high-resolution comparison between experiment and theory for a molecule−ion system.

The apparatus employed here is shown in the Supporting Information (SI) (Figure S1). Laser ablation of metallic Be is used to produce Be^+ ions, which are trapped in a linear radio frequency Paul trap.[30] Laser cooling[31] is used to cool the translational motion of the ions, resulting in a Coulomb crystal of Be^+ ions. Gaseous, room-temperature H_2O molecules are

Received: May 5, 2018
Accepted: June 12, 2018
Published: June 12, 2018

DOI: 10.1021/acs.jpclett.8b01437
J. Phys. Chem. Lett. 2018, 9, 3555−3560

then introduced via a leak valve into the trapping region, where they react with the trapped ions. Charged products of the chemical reaction remain in the trap and are subsequently detected via an integrated time-of-flight mass spectrometer (TOFMS) recently developed by our group[32,33] and used to discover new species.[34] The total reaction rate is measured by monitoring the decay of Be^+ ion fluorescence, and the product branching ratios are extracted from the mass spectrum.

A key feature of this experiment is that by varying the detuning of the 313 nm laser used to cool the ions, the population in the excited $1s^22p^1\ ^2P_{3/2}$ and ground $1s^22s^1\ ^2S_{1/2}$ states can be controlled. Because the energy difference between the ground and excited states is 3.96 eV, several more product channels are open for the $Be^+(^2P_{3/2}) + H_2O$ entrance channel. Using this system, we are able to measure the reaction rate and product branching ratio for these two entrance channels. We find that the ground-state channel, $Be^+(^2S_{1/2}) + H_2O$, exclusively produces $BeOH^+ + H$, whereas the excited-state channel, $Be^+(^2P_{3/2}) + H_2O$, also produces $H_2O^+ + Be$ with a yield of ∼10%. Specifically, the reactions considered here are

$$Be^+(^2S_{1/2}) + H_2O \rightarrow BeOH^+ + H \quad (1)$$

$$Be^+(^2P_{3/2}) + H_2O \rightarrow BeOH^+ + H \quad (2)$$

$$Be^+(^2P_{3/2}) + H_2O \rightarrow H_2O^+ + Be \quad (3)$$

$$H_2O + H_2O^+ \rightarrow H_3O^+ + OH \quad (4)$$

$$Be^+(^2P_{3/2}) + H_2O \rightarrow BeH^+ + OH \quad (5)$$

$$BeH^+ + H_2O \rightarrow BeOH^+ + H_2 \quad (6)$$

$$Be^+(^2P_{3/2}) + H_2O \rightarrow BeO^+ + H_2 \quad (7)$$

$$BeO^+ + H_2O \rightarrow BeOH^+ + OH \quad (8)$$

Because the translational energy of the laser-cooled Be^+ ions is <0.5 K, the energy of the room-temperature water sets the reaction kinetic energy of $Be^+ + H_2O$ in the center of mass frame to ∼100 K. The internal state distribution of the H_2O is assumed to be given by 300 K. Typical TOF traces (10 sample average) at reaction times t = 0 and 70 s with 7 and 26% relative $Be^+\ ^2P_{3/2}$ state excitation are shown in Figure 1A,B, respectively. The fluorescence signal, which is used to determine reaction time zero and normalize the initial ion number for the TOF, is monitored by the camera (ANDOR iXon3 EMCCD) in real time. At t = 0 s, a large peak of m/z = 9 (Be^+) and a smaller one of m/z = 26 ($BeOH^+$) are evidenced in the TOF trace (blue line), which indicates that Be^+ ions are the main species in the trap at t = 0. The finite amount of $BeOH^+$ at t = 0 reflects the fact that reactions 1−8 happen even during the loading process and that the mass filtering procedure is imperfect. At t = 70 s, a m/z = 19 peak emerges when more Be^+ ions are excited to $^2P_{3/2}$ state (1B), which we identify as H_3O^+ resulting from reactions 3 and 4. The $BeOH^+/H_3O^+$ ratio, $\eta(P_P)$, is measured by integrating both peaks for the experimentally controlled excited-state population P_P. The $BeOH^+$ signal includes the amount unfiltered during loading, products from both reactions 1 and 2, as well as, in principle, the two-step reactions 5 and 6 and 7 and 8. The H_3O^+ signal is produced via the two-step reactions 3 and 4. Whereas we do not observe products from reactions 5−8 (see also Figure S2 in the SI), they are thermochemically allowed and therefore included in our analysis, which sets upper limits on their reaction rate coefficients.

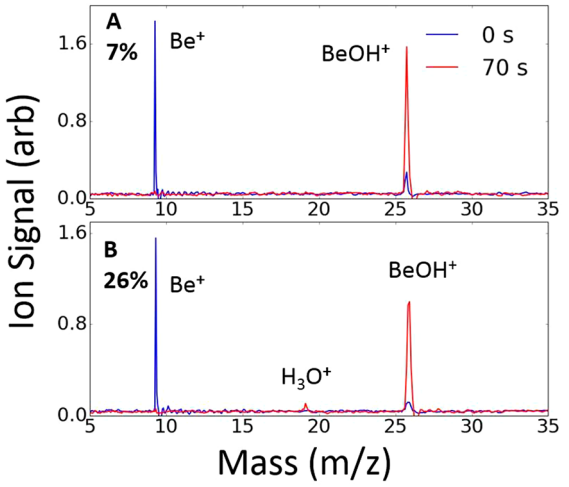

Figure 1. TOF signal (averaged over 10 trials) at reaction time t = 0 and 70 s with (A) P_P = 7% (A) and (B) P_P = 26%. A clear m/z = 19 peak emerges when more Be^+ ions are excited to $^2P_{3/2}$ state. The $BeOH^+/H_3O^+$ ratio for this case (P_P = 26%) is measured to be $\eta(0.26) = 0.039 \pm 0.006$ by integrating both peaks in B when t = 70 s.

The total reaction rate is given by $\Gamma_t = \rho_{H_2O}k_t$, where ρ_{H_2O} is the H_2O density measured from a Stanford Research Systems residual gas analyzer (RGA) calibrated to an ion gauge (see the SI for more information) and k_t is the total reaction rate coefficient. Because we have no conclusive detection of BeH^+ or BeO^+, k_t is approximated as $k_t = P_Sk_1 + P_Pk_2 + P_Pk_3$, where P_S and P_P are the Be^+ population in the $^2S_{1/2}$ and $^2P_{3/2}$ states, respectively, and k_i is the reaction rate coefficient of reaction i. Reaction 4 has been studied by other groups, reporting a rate coefficient of $(2.05 \pm 0.10) \times 10^{-9}$ cm^3/s.[35] The measured $H_3O^+/BeOH^+$ ratio is given from the reaction rates by

$$\eta(P_P) = \frac{P_Pk_3}{P_Sk_1 + P_Pk_2} \quad (9)$$

To use eq 9 to extract the individual rate coefficients (k_i), the total reaction rate Γ_t is first measured by monitoring the Be^+ fluorescence decay with a camera, as shown in Figure 2A (see also the SI). Fluorescence decay is monitored directly after a DC voltage applied to trap electrodes is used to filter out the heavier products from the trap to allow better crystallization of the Be^+ ions by reducing ion−ion heating.[36] The inset of Figure 2A shows typical fluorescence images of the Be^+ coulomb crystal at various times. Fluorescence is used to measure the total reaction rate because the total measurement time is ∼30 times shorter than using the TOFMS (Figure S2). To determine the separate rate coefficients for the Be^+ ground and excited states, we measure the total reaction rate coefficients for different excited-state fractions, shown in Figure 2B. A linear fit (blue line) is found using the least-squares method. The vertical intercept of this fit gives the Be^+ ground-state reaction rate coefficient $k_1 = (2.2 \pm 0.3_{stat}) \times 10^{-9}$ cm^3/s, whereas the sum of the slope and intercept gives the total excited-state Be^+ reaction rate coefficients $k_2 + k_3 = (4.7 \pm 1.7_{stat}) \times 10^{-9}$ cm^3/s. Using eq 9, the reaction rate coefficients of reactions 2 and 3 are then calculated to be $k_2 = (4.2 \pm 1.6_{stat}) \times 10^{-9}$ cm^3/s and $k_3 = (0.47 \pm 0.11_{stat}) \times 10^{-9}$ cm^3/s, respectively. The ratio of

DOI: 10.1021/acs.jpclett.8b01437
J. Phys. Chem. Lett. 2018, 9, 3555−3560

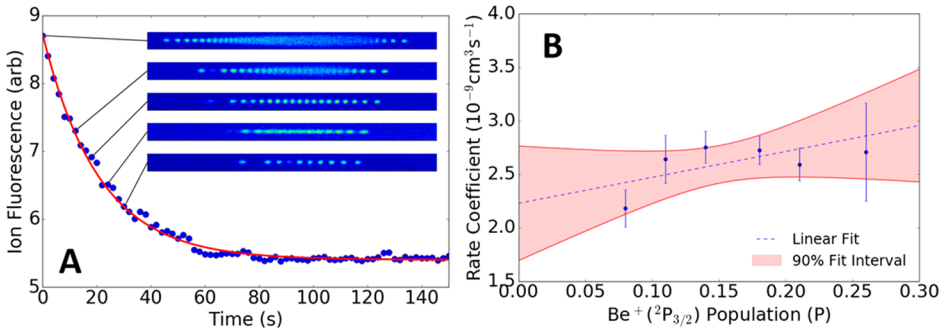

Figure 2. (A) Typical fluorescence decay measurement. The inset images are a subset of the original ion fluorescence images recorded by the camera. The red curve is an exponential fit (with a free offset) to the data, which gives the total reaction rate. (B) Total reaction rate coefficient as a function of Be$^+$(^{2}P$_{3/2}$) state population can be used to separate the contributions from the ground and excited states of Be$^+$.

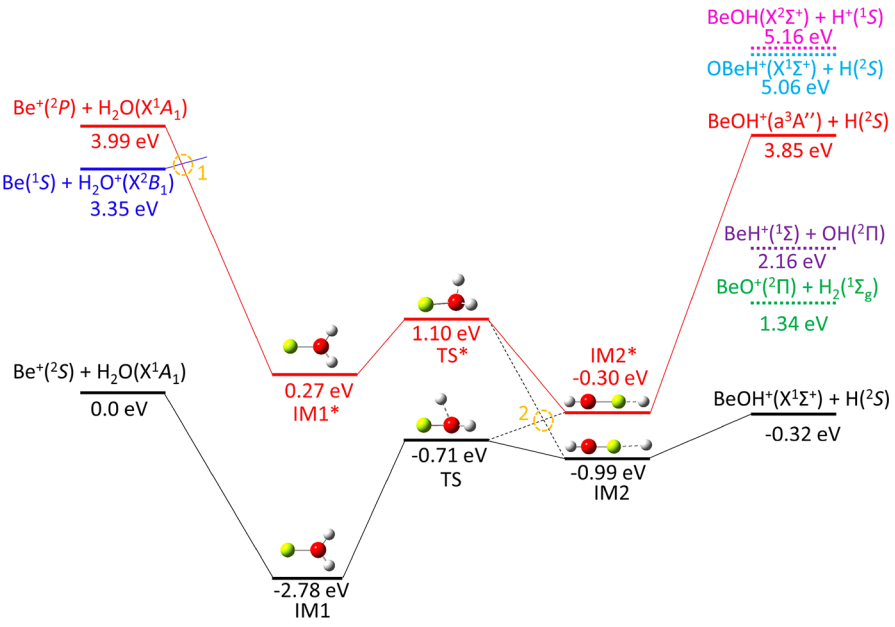

Figure 3. Energetics of both the ground- and excited-state reaction pathways for the Be$^+$ + H$_2$O reaction. Whereas reaction 1 proceeds on a single adiabatic PES, the reactions involving excited Be$^+$ depend on nonadiabatic transitions between different PESs (yellow circles). The two intersections, denoted as 1 and 2, are discussed in the text. The energetics of the stationary points of the excited-state PES were obtained by optimization at the CASSCF level followed by MRCI single-point calculations. Only one excited state is included in the Figure, but at least two are involved in the reactions. There is no zero-point correction here, but it does not change the overall energetics.

reaction rate coefficients for reactions 3 to 2 is therefore $k_3/k_2 = 0.11 \pm 0.03$ independent of systematic errors in the density measurement. Charged products from reactions 5 and 7 were not seen in this experiment despite both being thermochemically allowed. The absence of BeH$^+$ (reaction 5) and BeO$^+$ (reaction 7) products could be due to much higher reaction rates for reactions 6 and 8; by assuming that reactions 6 and 8 proceed at the capture rate, we set a 90% confidence bound on the reaction rate coefficients of reactions 5 and 7 to be $<5\times 10^{-10}$ cm^3/s. Reactions at these upper bounds for the rate coefficients do not significantly change the analysis above, justifying their exclusion from k_i.

It is instructive to compare these measured rate coefficients to those predicted by capture theory. For an ion reacting with a polar molecule, the leading order interaction potential as a function of the molecule−ion separation r is described by monopole−dipole interaction ($U \propto r^{-2}$) and the polarization of the molecule by the ion ($U \propto r^{-4}$). For this case, the rate coefficient is typically found using the average dipole orientation (ADO) collision model,[37] where the ion−dipole interaction is averaged over rotational states. The expression for the rate coefficient from ADO theory is

$$k_{\mathrm{ADO}} = 2\pi e\sqrt{\frac{\alpha}{\mu}} + 2\pi e\mu_{\mathrm{D}}C\sqrt{\frac{2}{\mu\pi kT}} \tag{10}$$

where α is the average neutral molecule polarizability, μ is the reduced mass, μ_{D} is the molecular dipole moment, e is the elementary charge, and C is the dipole locking constant. As a capture theory, ADO theory assumes that the reaction is dominated by long-range intermolecular forces, and when the ion moves inside the maximum of the centrifugal barrier, the reaction always proceeds with unit efficiency. The ADO model predicts that both the ground and excited Be$^+$ states react with a rate coefficient of 4.1×10^{-9} cm^3/s at 100 K reaction temperature, roughly two times larger than measured for the ground state, but in agreement with the measured reaction rate of the excited state. However, because it is long-range, the ADO model cannot provide the branching ratio and state-

DOI: 10.1021/acs.jpclett.8b01437
J. Phys. Chem. Lett. 2018, 9, 3555−3560

dependent information and is therefore insufficient for describing the observed reactions.

To further understand the mechanism of this reaction, a full-dimensional PES is constructed for the ground-state Be^+ reaction with H_2O. This PES consists of long-range and short-range terms, which are smoothly connected via a switching function. The long-range potential in the entrance channel contains the ion−dipole, ion-induced dipole, and ion−quadrupole interactions, whereas the short-range one is obtained by fitting ∼20 000 ab initio points calculated using an explicitly correlated unrestricted coupled cluster singles, doubles, and perturbative triples (UCCSD(T)-F12a)[38] with the specially optimized triple zeta correlation-consistent F12 basis set (VTZ-F12).[39] A high-fidelity fit was achieved using the permutation-invariant polynomial-neural network (PIP-NN) approach.[40] The details of the PES construction are given in the SI. The reaction path for reaction 1 is shown in Figure 3. It is clear from the Figure that the reaction is dominated by a deep potential well, which supports the formation of the Be−OH_2^+ reaction intermediate. However, there is a submerged barrier corresponding to a Be insertion into a O−H bond, shown as the transition state (TS) in Figure 3. On the other side of the barrier, there exists a collinear H−Be−O−H^+ well, which is much shallower than the Be−OH_2^+ well.

Although cold collisions should ideally be treated quantum mechanically,[41] it is still difficult to perform quantum scattering calculations for tetratomic systems, because of the long de Broglie wavelength in the scattering coordinate.[42] In this work, the rate coefficient of reaction 1 is computed on the PIP-NN PES using a quasi-classical trajectory (QCT) method. To mitigate the well-known zero-point energy (ZPE) violation in QCT method, we used the Paul−Hase method,[43] which turns back ZPE-violating trajectories by changing the sign of the momentum. ∼30 000 trajectories were computed with initial conditions that mimic the collision between H_2O at internal temperature of 300 K and Be^+ with a relative collision temperature of 100 K. The calculated rate coefficient is $(2.02 \pm 0.04) \times 10^{-9}$ cm^3/s, which is in good agreement with the experimental value. It is interesting to note that the capture rate coefficient under the same initial conditions, which is computed by counting trajectories that fall into the Be−OH_2^+ well, is significantly larger ($(3.31 \pm 0.05) \times 10^{-9}$ cm^3/s). This value is close to the ADO model, as it should be. The reduction of the rate in the QCT calculations suggests that some of the captured trajectories return to the reactant asymptote due to the bottleneck formed by the submerged barrier. Indeed, 38.7% of the captured trajectories eventually returned to the reactant asymptote. This can be regarded as a signature of dynamics.

To understand the reactivity and product branching for the $Be^+(^2P)$ + H_2O reaction, we have carried out complete active space self-consistent (CASSCF) calculations using the augmented correlation-consistent triple-ζ basis (aug-cc-pVTZ). As shown in Figure 4, the $A''(B_1)$ state from the $Be^+(^2P)$ + $H_2O(X^1A_1)$ asymptote forms an avoided crossing (denoted as 1 in Figure 3) with the $A''(B_1)$ electronic state correlated to $Be(^1S)$ + $H_2O^+(^2B_1)$. It also forms a conical intersection with the $A'(B_2)$ state. These two intersections apparently facilitate the charge-transfer process (reaction 3). In addition, a conical intersection (denoted as 2 in Figure 3) is found between an excited state and the ground electronic state that allows the formation of the $BeOH^+(X^1\Sigma^+)$ product (reaction 2). The branching between these two product

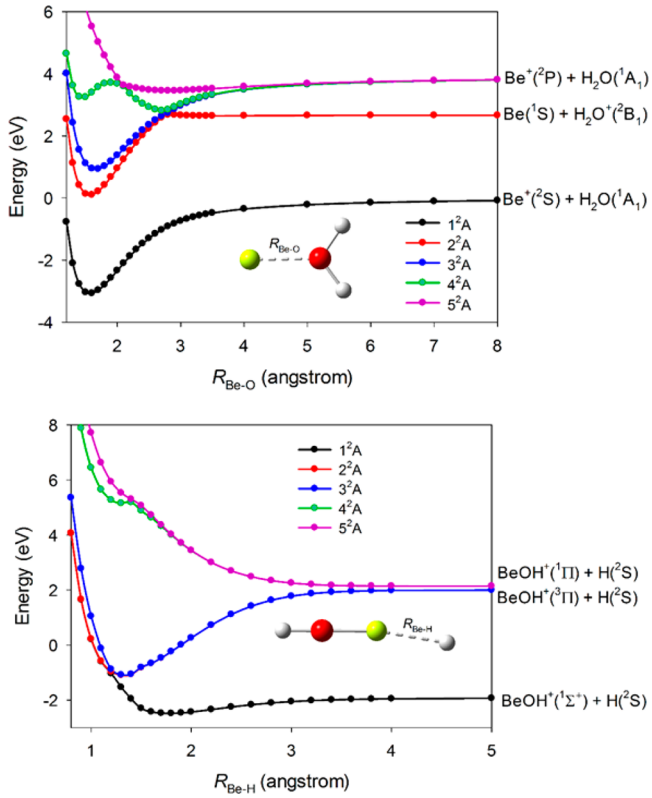

Figure 4. Potential energy curves for both the reactant and product channels computed at the CASSCF level. The C_{2v} symmetry is maintained in the upper panel, while a quasi-linear (∠O−Be−H = 175°) is kept in the lower panel to avoid complications in linearity.

channels thus depends on the interplay between these two nonadiabatic pathways. The stationary points along the reaction pathways have been further computed at the multireference configuration interaction (MRCI) level at the CASSCF geometries and are shown in Figure 3. Because of the complex electronic structures and nonadiabatic couplings, no global PESs have been developed. Nonadiabatic effects are not considered in the ground-state dynamics. It is nonetheless quite clear that the excited-state reaction is much more exothermic and less hindered by the analogous submerged barrier on the excited-state PES. As a result, its rate should essentially be collisional, consistent with the experimental result. More details of the ab initio calculations can be found in the SI.

To summarize, chemical reactions of laser-cooled Be^+ ions with room-temperature water vapor have been studied experimentally and theoretically for the first time. Ground-state Be^+ ions produce only $BeOH^+$ + H with a reaction rate coefficient of $k_1 = (2.2 \pm 0.3_{stat}) \times 10^{-9}$ cm^3/s, whereas the excited-state Be^+ not only creates $BeOH^+$ + H with a reaction rate coefficient of $k_2 = (4.2 \pm 1.6_{stat}) \times 10^{-9}$ cm^3/s but also gives H_2O^+ + Be with a reaction rate of $k_3 = (0.47 \pm 0.11_{stat}) \times 10^{-9}$ cm^3/s. Electronic structure calculations indicate that these two products are both produced via nonadiabatic pathways. The ground-state reaction rate is roughly half of that predicted by typically employed capture models but in good agreement with zero-point-corrected QCT calculations on an accurate full-dimensional global PES based on high-level ab initio calculations. These calculations reveal that the lower reaction rate is a consequence of chemical dynamics due to a

DOI: 10.1021/acs.jpclett.8b01437
J. Phys. Chem. Lett. 2018, 9, 3555−3560

submerged barrier in the product channel. In the future, we plan to study this reaction at the state-selective level at low temperature with a cryogenic buffer gas beam of H_2O.

■ ASSOCIATED CONTENT

Supporting Information

The Supporting Information is available free of charge on the ACS Publications website at DOI: 10.1021/acs.jpclett.8b01437.

Apparatus, pressure calibration, ground-state potential energy surface, QCT calculations, and reaction pathways (PDF)

■ AUTHOR INFORMATION

Corresponding Authors

*T.Y.: E-mail: yangtiangang@g.ucla.edu.
*A.L.: E-mail: liay@nwu.edu.cn.

ORCID

Tiangang Yang: 0000-0002-8940-8875
Anyang Li: 0000-0001-6634-842X
Arthur G. Suits: 0000-0001-5405-8361
Hua Guo: 0000-0001-9901-053X

Notes

The authors declare no competing financial interest.

■ ACKNOWLEDGMENTS

This work was funded by the Air Force Office of Scientific Research grant no. FA9550-16-1-0018. A.L. acknowledges the support of the National Natural Science Foundation of China (no. 21603174) and the Key Science and Technology Innovation Team of Shanxi Province (2017KCT-37). The UNM team acknowledges the Air Force Office of Scientific Research for funding (FA9550-15-1-0305). The calculations were performed at National Supercomputing Center in Shenzhen and Center for Advanced Scientific Computing Center at UNM. The UCLA authors thank Michael Jura for his encouragement to pursue ion−molecule chemistry.

■ REFERENCES

(1) Agúndez, M.; Wakelam, V. Chemistry of Dark Clouds: Databases, Networks, and Models. *Chem. Rev.* **2013**, *113*, 8710−8737.
(2) Krasnopolsky, V. A. Chemical Composition of Titan's Atmosphere and Ionosphere: Observations and the Photochemical Model. *Icarus* **2014**, *236*, 83−91.
(3) Adams, N. G.; Smith, D. The Selected Ion Flow Tube (SIFT); a Technique for Studying Ion-Neutral Reactions. *Int. J. Mass Spectrom. Ion Phys.* **1976**, *21*, 349−359.
(4) Armentrout, P. Reactions and Thermochemistry of Small Transition Metal Cluster Ions. *Annu. Rev. Phys. Chem.* **2001**, *52*, 423−461.
(5) Sims, I. R.; Smith, I. W. M. Gas-Phase Reactions and Energy Transfer at Very Low Temperatures. *Annu. Rev. Phys. Chem.* **1995**, *46*, 109−138.
(6) Smith, I. W. M.; Rowe, B. R. Reaction Kinetics at Very Low Temperatures: Laboratory Studies and Interstellar Chemistry. *Acc. Chem. Res.* **2000**, *33*, 261−268.
(7) Snow, T. P.; Bierbaum, V. M. Ion Chemistry in the Interstellar Medium. *Annu. Rev. Anal. Chem.* **2008**, *1*, 229−259.
(8) Gioumousis, G.; Stevenson, D. P. Reactions of Gaseous Molecule Ions with Gaseous Molecules. V. Theory. *J. Chem. Phys.* **1958**, *29*, 294−299.
(9) Mikosch, J.; Trippel, S.; Eichhorn, C.; Otto, R.; Lourderaj, U.; Zhang, J. X.; Hase, W. L.; Weidemuller, M.; Wester, R. Imaging Nucleophilic Substitution Dynamics. *Science* **2008**, *319*, 183−186.
(10) Li, A.; Li, Y.; Guo, H.; Lau, K.-C.; Xu, Y.; Xiong, B.; Chang, Y.-C.; Ng, C. Y. Communication: The Origin of Rotational Enhancement Effect for the Reaction of $H_2O^+ + H_2$ (D_2). *J. Chem. Phys.* **2014**, *140*, 011102.
(11) Carrascosa, E.; Meyer, J.; Wester, R. Imaging the Dynamics of Ion−Molecule Reactions. *Chem. Soc. Rev.* **2017**, *46*, 7498−7516.
(12) Xie, J.; Otto, R.; Mikosch, J.; Zhang, J.; Wester, R.; Hase, W. L. Identification of Atomic-Level Mechanisms for Gas-Phase $X^- + CH_3Y$ S_N2 Reactions by Combined Experiments and Simulations. *Acc. Chem. Res.* **2014**, *47*, 2960−2969.
(13) Clary, D. C. Fast Chemical Reactions: Theory Challenges Experiment. *Annu. Rev. Phys. Chem.* **1990**, *41*, 61−90.
(14) Hudson, E. R. Sympathetic Cooling of Molecular Ions with Ultracold Atoms. *EPJ. Technol. Instrum.* **2016**, *3:8*, 1−21.
(15) Tomza, M.; Jachymski, K.; Gerritsma, R.; Negretti, A.; Calarco, T.; Idziaszek, Z.; Julienne, P. Cold Hybrid Ion-Atom Systems. 2017, arXiv:physics/1708.07832. arXiv.org e-Print archive. https://arxiv.org/abs/1708.07832 (accessed Aug 5, 2018).
(16) Willitsch, S. Coulomb-Crystallised Molecular Ions in Traps: Methods, Applications, Prospects. *Int. Rev. Phys. Chem.* **2012**, *31*, 175−199.
(17) Highberger, J. L.; Savage, C.; Bieging, J. H.; Ziurys, L. M. Heavy-Metal Chemistry in Proto-Planetary Nebulae: Detection of MgNC, NaCN, and AlF toward CrRL 2688. *Astrophys. J.* **2001**, *562*, 790−798.
(18) Oppenheimer, M.; Dalgarno, A. The Fractional Ionization in Dense Interstellar Clouds. *Astrophys. J.* **1974**, *192*, 29−32.
(19) van Dishoeck, E. F.; Herbst, E.; Neufeld, D. A. Interstellar Water Chemistry: From Laboratory to Observations. *Chem. Rev.* **2013**, *113*, 9043−9085.
(20) Bollinger, J. J.; Wells, J. S.; Wineland, D. J.; Itano, W. M. Hyperfine Structure of the $2p^2P_{1/2}$ State in $^9Be^+$. *Phys. Rev. A: At., Mol., Opt. Phys.* **1985**, *31*, 2711−2714.
(21) Chen, K.; Sullivan, S. T.; Hudson, E. R. Neutral Gas Sympathetic Cooling of an Ion in a Paul Trap. *Phys. Rev. Lett.* **2014**, *112*, 143009.
(22) Roth, B.; Blythe, P.; Wenz, H.; Daerr, H.; Schiller, S. Ion-Neutral Chemical Reactions between Ultracold Localized Ions and Neutral Molecules with Single-Particle Resolution. *Phys. Rev. A: At., Mol., Opt. Phys.* **2006**, *73*, 042712.
(23) Larson, D. J.; Bergquist, J. C.; Bollinger, J. J.; Itano, W. M.; Wineland, D. J. Sympathetic Cooling of Trapped Ions: A Laser-Cooled Two-Species Nonneutral Ion Plasma. *Phys. Rev. Lett.* **1986**, *57*, 70−73.
(24) Schowalter, S. J.; Dunning, A. J.; Chen, K.; Puri, P.; Schneider, C.; Hudson, E. R. Blue-Sky Bifurcation of Ion Energies and the Limits of Neutral-Gas Sympathetic Cooling of Trapped Ions. *Nat. Commun.* **2016**, *7*, 12448.
(25) Li, J.; Jiang, B.; Guo, H. Spin-Orbit Corrected Full-Dimensional Potential Energy Surfaces for the Two Lowest-Lying Electronic States of FH_2O and Dynamics for the $F + H_2O \rightarrow HF + OH$ Reaction. *J. Chem. Phys.* **2013**, *138*, 074309.
(26) Song, H.; Guo, H. Vibrational and Rotational Mode Specificity in the $Cl + H_2O \rightarrow HCl + OH$ Reaction: A Quantum Dynamical Study. *J. Phys. Chem. A* **2015**, *119*, 6188−6194.
(27) Ray, A. W.; Ma, J.; Otto, R.; Li, J.; Guo, H.; Continetti, R. E. Effects of Vibrational Excitation on the $F + H_2O \rightarrow HF + OH$ Reaction: Dissociative Photodetachment of Overtone-Excited [F-H-OH]. *Chem. Sci.* **2017**, *8*, 7821−7833.
(28) Li, J.; Jiang, B.; Song, H.; Ma, J.; Zhao, B.; Dawes, R.; Guo, H. From Ab Initio Potential Energy Surfaces to State-Resolved Reactivities: $X + H_2O \leftrightarrow HX + OH$ [X = F, Cl, and $O(^3P)$] Reactions. *J. Phys. Chem. A* **2015**, *119*, 4667−4687.
(29) Xiao, C.; Xu, X.; Liu, S.; Wang, T.; Dong, W.; Yang, T.; Sun, Z.; Dai, D.; Xu, X.; Zhang, D. H.; et al. Experimental and Theoretical

DOI: 10.1021/acs.jpclett.8b01437
J. Phys. Chem. Lett. 2018, 9, 3555−3560

Differential Cross Sections for a Four-Atom Reaction: HD + OH → H_2O + D. *Science* **2011**, *333*, 440−442.
(30) Paul, W. Electromagnetic Traps for Charged and Neutral Particles. *Rev. Mod. Phys.* **1990**, *62*, 531−540.
(31) Wineland, D. J.; Itano, W. M. Laser Cooling of Atoms. *Phys. Rev. A: At., Mol., Opt. Phys.* **1979**, *20*, 1521−1540.
(32) Schowalter, S. J.; Chen, K.; Rellergert, W. G.; Sullivan, S. T.; Hudson, E. R. An Integrated Ion Trap and Time-of-Flight Mass Spectrometer for Chemical and Photo-Reaction Dynamics Studies. *Rev. Sci. Instrum.* **2012**, *83*, 043103.
(33) Schneider, C.; Schowalter, S. J.; Chen, K.; Sullivan, S. T.; Hudson, E. R. Laser-Cooling-Assisted Mass Spectrometry. *Phys. Rev. Appl.* **2014**, *2*, 034013.
(34) Puri, P.; Mills, M.; Schneider, C.; Simbotin, I.; Montgomery, J. A.; Côté, R.; Suits, A. G.; Hudson, E. R. Synthesis of Mixed Hypermetallic Oxide $BaOCa^+$ from Laser-Cooled Reagents in an Atom-Ion Hybrid Trap. *Science* **2017**, *357*, 1370−1375.
(35) Huntress, W. T.; Pinizzotto, R. F. Product Distributions and Rate Constants for Ion - Molecule Reactions in Water, Hydrogen Sulfide, Ammonia, and Methane. *J. Chem. Phys.* **1973**, *59*, 4742−4756.
(36) Chen, K.; Sullivan, S. T.; Rellergert, W. G.; Hudson, E. R. Measurement of the Coulomb Logarithm in a Radio-Frequency Paul Trap. *Phys. Rev. Lett.* **2013**, *110*, 173003.
(37) Su, T.; Bowers, M. T. Ion-Polar Molecule Collisions: The Effect of Ion Size on Ion-Polar Molecule Rate Constants; the Parameterization of the Average-Dipole-Orientation Theory. *Int. J. Mass Spectrom. Ion Phys.* **1973**, *12*, 347−356.
(38) Knizia, G.; Adler, T. B.; Werner, H.-J. Simplified CCSD(T)-F12 Methods: Theory and Benchmarks. *J. Chem. Phys.* **2009**, *130*, 054104.
(39) Peterson, K. A.; Adler, T. B.; Werner, H.-J. Systematically Convergent Basis Sets for Explicitly Correlated Wavefunctions: The Atoms H, He, B−Ne, and Al−Ar. *J. Chem. Phys.* **2008**, *128*, 084102.
(40) Jiang, B.; Li, J.; Guo, H. Potential Energy Surfaces from High Fidelity Fitting of Ab Initio Points: The Permutation Invariant Polynomial-Neural Network Approach. *Int. Rev. Phys. Chem.* **2016**, *35*, 479−506.
(41) Balakrishnan, N. Perspective: Ultracold Molecules and the Dawn of Cold Controlled Chemistry. *J. Chem. Phys.* **2016**, *145*, 150901.
(42) Zhang, D. H.; Guo, H. Recent Advances in Quantum Dynamics of Bimolecular Reactions. *Annu. Rev. Phys. Chem.* **2016**, *67*, 135−158.
(43) Paul, A. K.; Hase, W. L. Zero-Point Energy Constraint for Unimolecular Dissociation Reactions. Giving Trajectories Multiple Chances to Dissociate Correctly. *J. Phys. Chem. A* **2016**, *120*, 372−378.

DOI: 10.1021/acs.jpclett.8b01437
J. Phys. Chem. Lett. 2018, 9, 3555−3560